

# POINTWISE SHAPE-ADAPTIVE DCT FOR HIGH-QUALITY DEBLOCKING OF COMPRESSED COLOR IMAGES

*Alessandro Foi, Vladimir Katkovnik, and Karen Egiazarian*

Institute of Signal Processing, Tampere University of Technology  
P.O. Box 553, 33101, Tampere, Finland  
web: [www.cs.tut.fi/~foi](http://www.cs.tut.fi/~foi) email: [firstname.lastname@tut.fi](mailto:firstname.lastname@tut.fi)

## ABSTRACT

We present an high-quality image deblocking algorithm based on the shape-adaptive DCT (SA-DCT) [20, 21]. The SA-DCT is a low-complexity transform which can be computed on a support of arbitrary shape. This transform has been adopted by the MPEG-4 standard [13] and it is found implemented in modern video hardware.

The use of this shape-adaptive transform for denoising and deblurring has been recently proposed [5, 4, 6], showing a remarkable performance.

In this paper we discuss and analyze the use of this approach for the deblocking of block-DCT compressed images. Particular emphasis is given to the deblocking of highly-compressed color images.

Extensive simulation experiments attest the advanced performance of the proposed filtering method. The visual quality of the estimates is high, with sharp detail preservation, clean edges. Blocking and ringing artifacts are suppressed while salient image features are preserved. The SA-DCT filtering used for the chrominance channels allows to faithfully reconstruct the missing structural information of the chrominances, thus correcting color-bleeding artifacts.

## 1. INTRODUCTION

The new JPEG-2000 image compression standard solved many of the drawbacks of its predecessor. The use of a wavelet transform computed globally on the whole image, as opposed to the localized block-DCT (B-DCT) (employed e.g. by the classic JPEG), does not introduce any blocking artifacts and allows it to achieve a very good image quality even at high compression rates.

Unfortunately, this new standard has received so far only very limited endorsement from digital camera manufacturers and software developers. As a matter of fact, the classic JPEG still dominates the consumer market and the near-totality of pictures circulated on the internet is compressed using this old standard. Moreover, the B-DCT is the work-horse on which even the latest MPEG video coding standards rely upon. There are no convincing indicators suggesting that the current trend is about to change any time soon. All these facts, together with the ever growing consumer demand for high quality imaging, makes the development of advanced and efficient post-processing (deblocking, deringing, etc.) techniques a very actual and relevant application area.

In this paper we propose a novel method for the restoration of B-DCT compressed grayscale and color images. It is based on the *pointwise shape-adaptive DCT (SA-DCT)* [5] approach and its characterized by a high quality of the filtered estimate.

The SA-DCT [20, 21] is a generalization of the usual separable block-DCT (B-DCT) which can be computed on a support of arbitrary shape. It is obtained by cascaded application of one-dimensional varying-length DCT transforms first on the columns and then on the rows that constitute the considered support. Thus, it retains the same computational complexity of the B-DCT. The

SA-DCT has been originally developed for coding non-rectangular image patches near the border of image objects, in such a way to minimize the stored information and to avoid the ringing artifacts (Gibbs phenomenon) that would appear in correspondence with strong edges. Because of its low-complexity, the near-optimal decorrelation and energy compaction properties (e.g. [20],[11]), and its backward-compatibility with the B-DCT, the SA-DCT has been included in the MPEG-4 standard [13], where it is used for the coding of image segments that lie on the video-object's boundary. The recent availability of low-power hardware SA-DCT platforms (e.g. [2],[12]) makes this transform an appealing choice for many image- and video-processing tasks.

The first attempt to use of SA-DCT for image denoising was reported by the authors in [5]. The original version of the method has been refined and a shape-adaptive transform-domain deconvolution filter for image deblurring has also been developed [4]. Further, a color version of the denoising algorithm has been proposed [6]. These denoising and deblurring algorithms demonstrate a remarkable performance, typically outperforming the best methods known to the authors. The SA-DCT estimates have also been shown (by an independent research) to achieve one of the highest subjective visual quality [22].

The paper is organized as follows. In the next section we give a brief overview on the basic anisotropic LPA-ICI + SA-DCT method. In Section 3 we discuss the adaptation of the denoising algorithm to deblocking and relate the quantization table with the value of the variance to be used for the filtering. The extension to color images and the "luminance-chrominance structural constraint" are the subject of Section 4. The final Section 5 is devoted to extensive experimental results: we consider different types of quantization tables, several level of compression, for grayscale as well as for color images.

## 2. ANISOTROPIC LPA-ICI-DRIVEN SA-DCT DENOISING

Here we give only a brief overview on the original method developed for image denoising and refer the reader to [4] (and references therein) for a more formal, complete, and rigorous description.

The use of a transform with a shape-adaptive support involves actually two separate problems: not only the transform should adapt to the shape (i.e. a shape-adaptive transform), but the shape itself must adapt to the image features (i.e. an adaptive shape). The first problem has found a very satisfactory solution in the SA-DCT transform [20, 21]. The second problem is essentially application-dependant. It must be noted that conventional segmentation (or local-segmentation) techniques which are employed for video processing (e.g. [17]) are not suitable for degraded (noisy, blurred, highly compressed, etc.) data. In our approach, we use the SA-DCT in conjunction with the anisotropic LPA-ICI technique [10, 9, 7]. By comparing varying-scale directional kernel estimates, the technique adaptively selects, for each point in the image, a set of directional adaptive-scales. The length of the support of the corresponding adaptive-scale kernels define the shape of the transform's support in a pointwise-adaptive manner. Examples of such neighborhoods are shown in Figure 4.

---

This work was partially supported by the Academy of Finland, project No. 213462 (Finnish Centre of Excellence program 2006 - 2011).



Figure 1: Details of the JPEG-compressed grayscale *Lena* ( $Q=6$ ,  $\text{bpp}=0.15$ ,  $\text{PSNR}=28.24\text{dB}$ ) and of the corresponding Pointwise SA-DCT estimate ( $\text{PSNR}=29.87\text{dB}$ ). The estimated standard deviation for this highly compressed image is  $\sigma=17.6$ .

For each one of these neighborhoods a SA-DCT is performed. The hard-thresholded SA-DCT coefficients are used to reconstruct a local estimate of the signal within the adaptive-shape support. By using the adaptive neighborhoods as support for the SA-DCT, we ensure that data are represented sparsely in the transform domain, allowing to effectively separate signal from noise using hard-thresholding.

Since supports corresponding to different points are in general overlapping (and thus generate an overcomplete representation of the signal), the local estimates are averaged together using adaptive weights that depend on the local estimates' statistics. In this way we obtain and adaptive estimate of the whole image.

Once this global estimate is produced, it can also be used as reference estimate for an empirical Wiener filter in SA-DCT domain. Following the same adaptive averaging procedure as for hard-thresholding, we arrive to the final Anisotropic LPA-ICI-driven SA-DCT estimate. We call this procedure “*Pointwise SA-DCT*”.

We remark that the LPA-ICI technique is fast, since it is based on convolutions against one-dimensional kernels for a very limited number of directions. It constitutes a negligible overhead for the whole SA-DCT filtering algorithm.

### 3. POINTWISE SA-DCT FOR B-DCT ARTIFACTS REMOVAL

While more sophisticated models of B-DCT-domain quantization noise have been proposed by many authors, we model this degradation as some additive Gaussian white noise. In this section we restrict our attention to the grayscale/single-channel case and thus assume the observation model

$$z = y + n, \quad (1)$$

where  $y$  is the original (non-compressed) image,  $z$  its observation after quantization in B-DCT domain, and  $n$  is independent Gaussian with variance  $\sigma^2$ ,  $n(\cdot) \sim \mathcal{N}(0, \sigma^2)$ .

We estimate a suitable value for the variance  $\sigma^2$  directly from the quantization table  $\mathbf{Q} = [q_{i,j}]_{i,j=1,\dots,8}$  using the following empirical formula:

$$\sigma^2 = 0.69 \cdot \left( \frac{1}{9} \sum_{i,j=1}^3 q_{i,j} \right)^{1.3}. \quad (2)$$

This formula uses only the mean value of the nine table entries which correspond to the lowest-frequency DCT harmonics (including the DC-term) and has been experimentally verified to be quite robust for a wide range of different quantization tables and images. A higher compression obviously corresponds to a larger value for the variance.

Note that the  $\sigma^2$  which is calculated by (2) is *not* an estimate of the variance of compressed image, *nor* it is an estimate of the variance of the difference between original and compressed images.



Figure 2: Details of the JPEG-compressed *Lena* ( $Q=15$ ,  $\text{bpp}=0.29$ ,  $\text{PSNR}=31.95\text{dB}$ ) and of the corresponding Pointwise SA-DCT estimate ( $\text{PSNR}=33.21\text{dB}$ ). The estimated standard deviation for this compressed image is  $\sigma=9.7$ .

Instead, it is simply the variance of the white Gaussian noise  $n$  in the observation model (1). Roughly speaking, it is the variance of some hypothetical noise which, if added to the original image  $y$ , would require – in order to be removed – the same level of adaptive smoothing which is necessary to suppress the artifacts generated by the B-DCT quantization with the table  $\mathbf{Q}$ .

Figures 1 and 2 show fragments of the JPEG-compressed grayscale *Lena* image obtained for two different compression levels (JPEG quality  $Q=6$  and  $Q=15$ ) and the corresponding SA-DCT filtered estimates. For these two cases the estimated standard deviations are  $\sigma=17.6$  and  $\sigma=9.7$ .

Let us observe that the procedure defined by (2) can be used in a straightforward manner, because the quantization tables are always (and necessarily) either provided with the coded data, or fixed in advance by the compression standard. It allows to apply the Pointwise SA-DCT denoising algorithm [4] as an effective deblocking and de-ringing filter for B-DCT coded images and videos. The proposed method is particularly relevant for video post-processing, since it can exploit the SA-DCT hardware of MPEG-4 decoders.

### 4. COLOR IMAGE PROCESSING WITH STRUCTURAL CONSTRAINT IN LUMINANCE-CHROMINANCE SPACE

When compressing color images or video, the standard approach (e.g. in the JPEG and MPEG), is to first perform the  $YUV$  color transformation – which decomposes the signal in one luminance and two chrominance channels – and then process the resulting three channels separately. According to the modeling in the previous section, we assume that the original (non-compressed) image  $y = [y_R, y_G, y_B]$  in the  $RGB$  color space is represented, after B-DCT quantization in  $YUV$  space as

$$z_C = y_C + n_C, \quad C = Y, U, V,$$

where  $y_Y, y_U$  and  $y_V$  are the luminance and chrominance channels of  $y$ ,  $z_Y, z_U$  and  $z_V$  are the corresponding channels after quantization in B-DCT domain, and  $n = [n_Y, n_U, n_V]$  is independent Gaussian noise,  $n_C(\cdot) \sim \mathcal{N}(0, \sigma_C^2)$ .

We estimate the variances  $\sigma_Y^2$ ,  $\sigma_U^2$ , and  $\sigma_V^2$  from the corresponding quantization tables for the luminance and chrominance channels, using formula (2). However, if – as it is commonly done – the chrominance channels are downsampled, then the estimated variances for the chrominances need to be further multiplied by 2, in order to take into account for the coarser sampling.

Usually, the quantization tables  $\mathbf{Q}^U$  and  $\mathbf{Q}^V$  used for the two chrominances coincide,  $\mathbf{Q}^U = \mathbf{Q}^V = \mathbf{Q}^{UV}$ . Following established models of the human visual system, a higher compression is performed on the chrominances than on the luminance. Thus, it is typical that the estimated variances are such that  $2\sigma_Y^2 < \sigma_U^2 = \sigma_V^2$ .

We give a first example of the proposed method for color images in Figure 3. In this example, the values of  $\sigma_Y$  and  $\sigma_U = \sigma_V$  calculated according to formula (2) are 12.6 and 27.1, respectively.

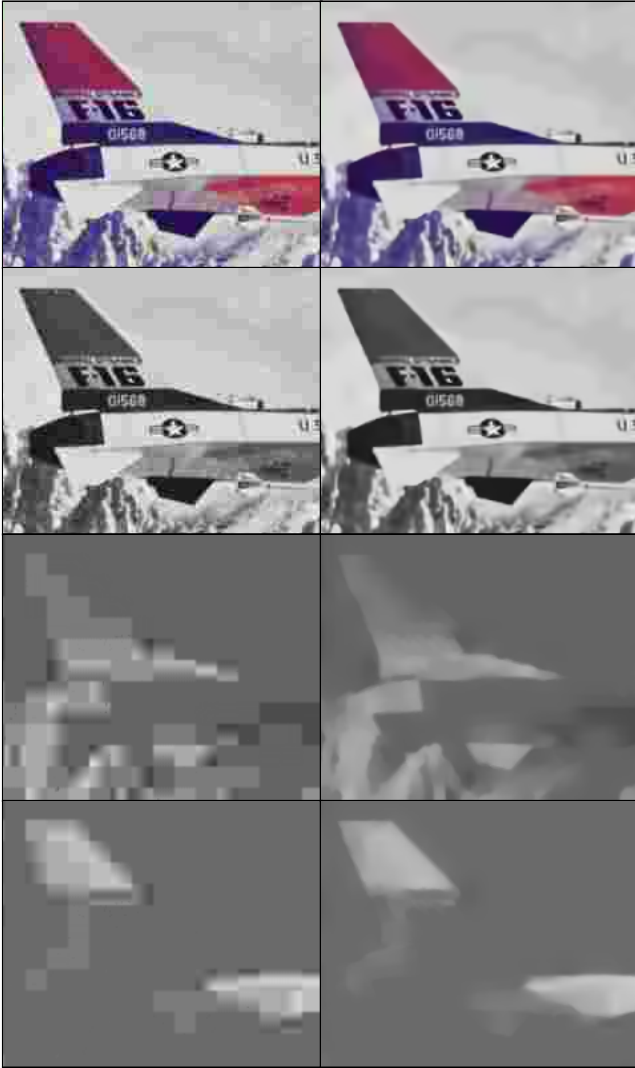


Figure 3: Fragments of the JPEG-compressed ( $Q=10$ ,  $0.25\text{bpp}$ ,  $PSNR=26.87\text{dB}$ ), and restored *F-16* image ( $PSNR=28.30\text{dB}$ ). Top to bottom row: *RGB* color, luminance  $Y$ , and chrominance  $U$  and  $V$  channels.

As proposed in [6] for color image denoising, we approach color data in a channel-by-channel manner imposing a unique structural constraint among the three channels. This allows to filter the chrominance channels restoring the structural information which went lost because of quantization and coarse sampling. The peculiarity of our approach is easily explained and demonstrated through this first example.

Even at relatively high bit-rates, the compression of the chrominance channels is usually quite aggressive. The typical scenario is illustrated in Figure 3. It can be seen that only very few *AC*-terms of the chrominance blocks survive to quantization, and the resulting chrominance channels end up with the vast majority of blocks represented by the *DC*-term only. It results in unpleasant color-bleeding artifacts along edges between differently colored objects. At the same time, on smoother areas the uneven hue due to quantization becomes particularly noticeable.

Ideally, the  $Y$ ,  $U$ , and  $V$  channels are considered as independent. Therefore, the common approach is to filter the three channels separately and independently one from the other.

However, when considering natural images, the different color channels typically share some common features which are inherited from the structures and from the objects depicted in the original image. In particular, it can be observed that along the objects' bound-

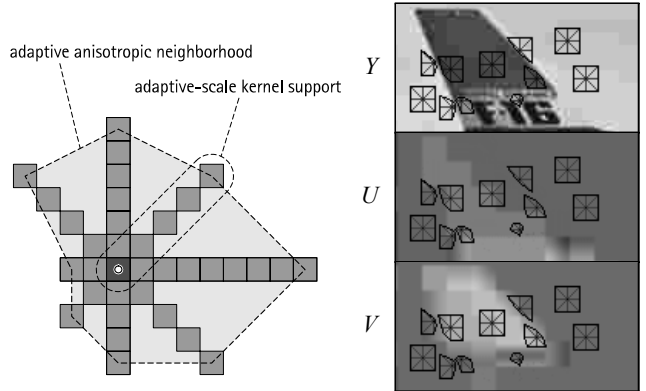


Figure 4: The anisotropic neighborhood is constructed as the polygonal hull of the adaptive-scale directional kernels supports (left). The adaptive anisotropic neighborhoods are selected by the *LPA-ICI* on the luminance channel (right-top). Observe that the neighborhoods are not affected by the blocking artifacts and yet are quite accurate with respect to the image features. These neighborhoods are used for *SA-DCT* filtering of the luminance as well as of the two chrominances (right-middle and right-bottom). The result of such filtering is shown in the right column of Figure 3.

aries all color channels of the original image usually exhibit some simultaneous discontinuities or sharp transitions.

We exploit this kind of structural correlation by imposing that the three transform's supports which are used for the filtering of the  $Y$ ,  $U$ , and  $V$  channels at a particular location have the same adaptive shape. As shown in Figure 4(right), we use for all three channels the adaptive neighborhoods defined by the anisotropic *LPA-ICI* for the  $Y$  channel, because it is in the luminance that the structural information is usually better preserved after compression.

Such a constraint make so that whenever some structure is detected (by the *LPA-ICI*), it is taken into account (and thus preserved) for the filtering of all three channels. Restricted to the adaptive supports, however, the channels are assumed as independent, and thus the transform-domain filtering is still performed for each channel independently from the others.

Figure 3 shows that the proposed method effectively attenuates ringing and blocking artifacts, faithfully preserving the structures and the salient feature in the image. Moreover, it demonstrates its ability of *reconstructing the missing structural information* in the chrominance channels, where the details of the tail of the plane are clearly revealed, with precise boundaries. The obtained color estimate is then quite sharp, with well-defined edges, and the color-bleeding artifacts – obviously visible in the JPEG-compressed image – are accurately corrected.

## 5. EXPERIMENTAL RESULTS

In order to assess the filtering performance of the proposed method, extensive simulation experiments were carried out. We dedicated considerable effort in reproducing the same experimental settings used by other authors. This has not been always easy, since different authors consider different *B-DCT* quantizations tables, compression levels, and different images. Consequently, we present comparative numerical results collected in three separate tables. The first two tables contain results for grayscale images obtained using particular quantization tables found in the literature (Table 1) and JPEG (Table 2). The third and last table is dedicated to experiments with JPEG compression of color images.

Three quantization tables – usually called **Q1**, **Q2**, and **Q3** – have been used by many authors (e.g. [14] and references therein) in order to simulate various types of *B-DCT* compression. To help the reader identifying the considered quantization tables, we report

Table	Lena			Peppers			Barbara		
	image	others	SA-DCT	image	others	SA-DCT	image	others	SA-DCT
Q1	30.70	31.63	<b>32.12</b>	30.42	31.33	<b>32.02</b>	25.94	26.64	<b>26.79</b>
Q2	30.09	31.19	<b>31.56</b>	29.82	30.97	<b>31.45</b>	25.59	26.32	<b>26.45</b>
Q3	27.38	28.65	<b>29.03</b>	27.22	28.55	<b>29.13</b>	24.03	24.73	<b>25.13</b>

Table 1: PSNR comparison table for restoration from B-DCT quantization for three different quantization matrices. The values under “others” correspond to the best results of any of the methods [14, 8, 16, 18, 26, 24], as reported in [14].

here the first row of each table:

$$\mathbf{Q1}(1 \cdots 8, 1) = [50 \ 60 \ 70 \ 70 \ 90 \ 120 \ 255 \ 255],$$

$$\mathbf{Q2}(1 \cdots 8, 1) = [86 \ 59 \ 54 \ 86 \ 129 \ 216 \ 255 \ 255],$$

$$\mathbf{Q3}(1 \cdots 8, 1) = [110 \ 130 \ 150 \ 192 \ 255 \ 255 \ 255 \ 255].$$

The values of the standard deviation  $\sigma$  corresponding to these three tables – calculated using formula (2) – are 12.62, 13.21, and 22.73, respectively. In terms of image degradation, they correspond to a medium to high compression level, similar to what can be obtained by using JPEG with  $Q = 11$  (Q1),  $Q = 9$  (Q2), or  $Q = 5$  (Q3).

In Table 1 we present results for deblocking from B-DCT quantization performed using these specific quantization tables. We compare the results obtained by our SA-DCT algorithm against the best results obtained by any of the methods [14, 8, 16, 18, 26, 24], as reported in [14]. The results are in favor of our proposed technique, which consistently outperforms all other methods.

Further positive results are shown in Table 2 for the case of deblocking from JPEG-compression. In this second table we compare against the best result obtained by any of the methods [1, 3, 19, 25, 15, 16], as reported in [1]. Also in this comparison, the Pointwise SA-DCT method is found to be superior to all other techniques, outperforming them of about 0.5dB in all experiments.

In Table 3 we show results for the Pointwise SA-DCT filtering of JPEG-compressed color images, from very high ( $Q=4$ ) to very low ( $Q=50$ ) compression levels. It can be seen that the improvement is significant especially for very high and moderate compression levels. For very low compression levels – for which the compression artifacts are barely visible and thus there is typically no need for postprocessing – the improvement is still substantial for those images which present some structures or edges.

For the simulations in Table 2 and Table 3 as well as for all JPEG experiments presented in this paper, we use the baseline IJG JPEG implementation. For a JPEG-quality parameter  $Q=50$ , the top rows of the quantization tables for the luminance and chrominance channels are

$$\mathbf{Q}_{Q=50}^Y(1 \cdots 8, 1) = [16 \ 11 \ 10 \ 16 \ 24 \ 40 \ 51 \ 61],$$

$$\mathbf{Q}_{Q=50}^{UV}(1 \cdots 8, 1) = [17 \ 18 \ 24 \ 47 \ 99 \ 99 \ 99 \ 99],$$

and the corresponding estimated standard deviations according to (2) are  $\sigma_Y = 4.4$  and  $\sigma_U = \sigma_V = 9.7$ .

Figure 5 provides a further example of the accuracy of the proposed method. First, one can see the sharp reconstruction of contours (e.g. in the legs, shoulders and head). Color-bleeding and blocking artifacts are completely suppressed, not only on smooth regions but even on rather thin details such as the snorkel. Second, the figure shows that the method is still reliable even when no useful structural information can be extracted from the luminance channel. In particular, it can be seen that the swimsuit is composed of three differently colored patches, all of which have the same luminance. This makes impossible to reconstruct the boundaries between these patches in a very sharp manner, as the only information available lies in the chrominances. Nevertheless, because the SA-DCT is a basis (complete system), the different colors of these patches are well preserved, while the transform-domain thresholding effectively suppresses the blockiness.

More simulation results and the MATLAB software which implements the presented method are available at <http://www.cs.tut.fi/~foi/SA-DCT/>.

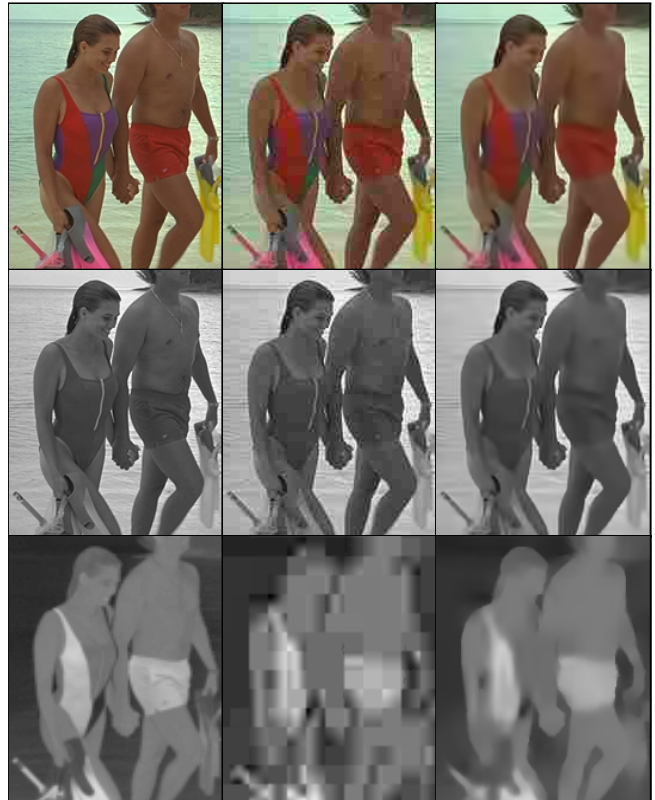


Figure 5: Fragments of the original, compressed, and restored Kodak image 12. Top to bottom row: RGB color, luminance  $Y$  channel, chrominance  $V$  channel. From left to right: original image, JPEG-compressed ( $Q=16$ , 0.25bpp,  $PSNR=30.45$ ), restored by proposed Pointwise SA-DCT method ( $PSNR=31.45$ ).

## REFERENCES

- [1] Averbuch, A., A. Schclar, and D.L. Donoho, “Deblocking of block-transform compressed images using weighted sums of symmetrically aligned pixels”, *IEEE Trans. Image Process.*, vol. 14, no. 2, pp. 200-212, February 2005.
- [2] Chen, K.-H., J. Guo, J.-S. Wang, C.-W. Yeh, and J.-W. Chen, “An energy-aware IP core design for the variable-length DCT/IDCT targeting at MPEG4 shape-adaptive transforms”, *IEEE Trans. Circuits and Systems for Video Technology*, vol. 15, no. 5, pp. 704-714, May 2005.
- [3] Chen, T., H.R. Wu, and B. Qiu, “Adaptive postfiltering of transform coefficients for the reduction of blocking artifacts”, *IEEE Trans. Circuits and Systems for Video Technology*, vol. 11, no. 5, pp. 584-602, August 2001.
- [4] Foi, A., K. Dabov, V. Katkovnik, and K. Egiazarian, “Shape-adaptive DCT for denoising and image reconstruction”, *Proc. SPIE El. Imaging 2006, Image Process.: Algorithms and Systems V*, 6064A-18, January 2006.
- [5] Foi, A., V. Katkovnik, and K. Egiazarian, “Pointwise shape-adaptive DCT as an overcomplete denoising tool”, *Proc. 2005 Int. TICSP Workshop Spectral Meth. Multirate Signal Process., SMMSP 2005*, pp. 164-170, Riga, June 2005.
- [6] Foi, A., V. Katkovnik, and K. Egiazarian, “Pointwise shape-adaptive DCT denoising with structure preservation in luminance-chrominance space”, *Proc. of the 2nd International Workshop on Video Processing and Quality Metrics for Consumer Electronics, VPQM2006*, Scottsdale, AZ, January 2006.
- [7] Goldenshluger, A., and A. Nemirovski, “On spatial adaptive estimation of nonparametric regression”, *Math. Meth. Statistics*, vol.6, pp.135-170, 1997.
- [8] Hsung, T.-C., and D.P.-K. Lun, “Application of singularity de-

Qual.	Lena			"Green Peppers" <sup>1</sup>			Barbara		
	JPEG (bpp)	others	SA-DCT	JPEG (bpp)	others	SA-DCT	JPEG (bpp)	others	SA-DCT
4	26.46 (0.11)	27.63	<b>28.08</b>	25.61 (0.14)	26.72	<b>27.41</b>	23.48 (0.14)	24.13	<b>24.65</b>
6	28.24 (0.15)	29.22	<b>29.87</b>	27.32 (0.18)	28.22	<b>28.97</b>	24.50 (0.18)	25.08	<b>25.51</b>
8	29.47 (0.18)	30.37	<b>30.99</b>	28.40 (0.22)	29.28	<b>29.90</b>	25.19 (0.23)	25.71	<b>26.11</b>
10	30.41 (0.22)	31.17	<b>31.84</b>	29.16 (0.25)	29.94	<b>30.51</b>	25.79 (0.28)	26.27	<b>26.61</b>
12	31.09 (0.25)	31.79	<b>32.48</b>	29.78 (0.28)	30.47	<b>31.00</b>	26.33 (0.32)	26.81	<b>27.10</b>

Table 2: PSNR comparison table from JPEG compression of grayscale images. The values under "others" correspond to the best result obtained by any of the methods [1, 3, 19, 25, 15, 16], as reported in [1].

Qual.	RGB Lena 512x512x24			RGB Peppers 512x512x24			RGB Baboon 512x512x24			RGB House 256x256x24		
	JPEG (bpp)	SA-DCT	ISNR	JPEG (bpp)	SA-DCT	ISNR	JPEG (bpp)	SA-DCT	ISNR	JPEG (bpp)	SA-DCT	ISNR
4	23.34 (0.12)	24.79	1.45	22.32 (0.13)	23.77	1.46	19.28 (0.17)	20.00	0.72	22.63 (0.15)	23.76	1.13
6	25.52 (0.16)	27.09	1.57	23.99 (0.17)	25.54	1.54	20.38 (0.26)	21.05	0.67	24.41 (0.19)	25.66	1.24
8	26.64 (0.19)	28.16	1.52	24.99 (0.21)	26.40	1.41	21.12 (0.35)	21.71	0.59	25.16 (0.24)	26.41	1.25
10	27.53 (0.23)	29.06	1.53	25.77 (0.25)	27.11	1.34	21.63 (0.43)	22.13	0.50	26.25 (0.27)	27.54	1.29
15	28.97 (0.31)	30.33	1.35	26.88 (0.33)	27.99	1.11	22.49 (0.62)	22.88	0.38	27.52 (0.34)	28.66	1.14
20	29.83 (0.38)	31.00	1.17	27.57 (0.40)	28.53	0.96	23.07 (0.77)	23.37	0.31	27.87 (0.41)	28.75	0.88
25	30.44 (0.44)	31.46	1.02	28.04 (0.47)	28.90	0.86	23.50 (0.92)	23.75	0.25	28.55 (0.47)	29.44	0.89
30	30.91 (0.50)	31.79	0.88	28.40 (0.54)	29.14	0.74	23.85 (1.05)	24.06	0.21	28.96 (0.54)	29.76	0.80
40	31.54 (0.61)	32.26	0.72	28.83 (0.66)	29.45	0.62	24.40 (1.29)	24.56	0.16	29.51 (0.65)	30.20	0.69
50	32.02 (0.72)	32.63	0.61	29.25 (0.78)	29.81	0.56	24.85 (1.51)	24.97	0.12	29.80 (0.76)	30.40	0.60

Table 3: PSNR (dB) results for the Pointwise SA-DCT filtering of JPEG-compressed color images. Results are given also in terms of improvement-in-SNR (ISNR, dB).

- tection for the deblocking of JPEG decoded images", *IEEE Trans. Circuits and Systems II*, vol. 45, no. 5, pp. 640-644, May 1998.
- [9] Katkovnik V., "A new method for varying adaptive bandwidth selection", *IEEE Trans. on Signal Proc.*, vol. 47, no. 9, pp. 2567-2571, 1999.
- [10] Katkovnik V., A. Foi, K. Egiazarian, and J. Astola, "Directional varying scale approximations for anisotropic signal processing," *Proc. of XII European Signal Process. Conf., EU-SIPCO 2004*, pp. 101-104, Vienna, September 2004.
- [11] Kauff, P., and K. Schuur, "Shape-adaptive DCT with block-based DC separation and  $\Delta$ DC correction", *IEEE Transactions on Circuits and Systems for Video Technology*, vol. 8, no. 3, pp. 237-242, 1998.
- [12] Kinane, A., A. Casey, V. Muresan, and N. O'Connor, "FPGA-based conformance testing and system prototyping of an MPEG-4 SA-DCT hardware accelerator", *IEEE 2005 Int. Conf. on Field-Programmable Technology, FPT' 05*, Singapore, December 2005.
- [13] Koenen, R., "Overview of the MPEG-4 Standard", ISO/IEC JTC1/SC29/WG11 Doc. N3536, July 2000.
- [14] Liew, A.W.C., and H. Yan, "Blocking Artifacts Suppression in Block-Coded Images Using Overcomplete Wavelet Representation", *IEEE Trans. Circuits and Systems for Video Technology*, vol. 14, no. 4, pp. 450-461, April 2004.
- [15] Marsi, S., R. Castagno, and G. Ramponi, "A simple algorithm for the reduction of blocking artifacts in images and its implementation", *IEEE Trans. Consum. Electron.*, vol. 44, no. 3, pp. 1062-1070, August 1998.
- [16] "MPEG-4 video verification model version 18.0 (VM-18)", ISO/IEC JTC1/SC29/WG11, Doc. N3908, 2001.
- [17] O'Connor, N., S. Sav, T. Adamek, V. Mezaris, I. Kompatsiaris, T.Y. Lu, E. Izquierdo, C. Bennström, and J. Casas, "Region and object segmentation algorithms in the Quimera segmentation platform", *Proc. Third Int. Workshop on Content-Based Multimedia Indexing (CBMI03)*, Rennes, pp. 381-388, 2003.
- [18] Paek H., R.C. Kim, and S.U. Lee, "On the POCS-based post-processing technique to reduce blocking artifacts in transform coded images," *IEEE Trans. Circuits Sys. Video Technology*, vol. 8, pp. 358-367, June 1998.
- [19] Rosenholts, R., and A. Zakhor, "Iterative procedures for reduction of blocking artifacts in transform domain image coding", *IEEE Trans. Circuits and Systems for Video Technology*, vol. 2, no. 2, pp. 91-95, March 1992.
- [20] Sikora, T., "Low complexity shape-adaptive DCT for coding of arbitrarily shaped image segments", *Signal Process.: Image Comm.*, vol. 7, pp. 381-395, 1995.
- [21] Sikora, T., and B. Makai, "Shape-adaptive DCT for generic coding of video", *IEEE Trans. Circuits and Systems for Video Techn.*, vol. 5, no. 1, pp. 59-62, 1995.
- [22] Van der Weken, D., E. Kerre, E. Vansteenkiste, and W. Philips, "Evaluation of fuzzy image quality measures using a multidimensional scaling framework" *Proc. of the 2nd Int. Workshop on Video Process. and Quality Metrics for Consumer Electronics, VPQM2006*, Scottsdale, AZ, January 2006.
- [23] Wu, S., H. Yan, and Z. Tan, "An efficient wavelet-based deblocking algorithm for highly compressed images", *IEEE Trans. Circuits and Systems for Video Technology*, vol. 11, no. 11, pp. 1193-1198, November 2001.
- [24] Xiong, Z., M. Orchard, and Y. Zhang, "A deblocking algorithm for JPEG compressed images using overcomplete wavelet representations", *IEEE Trans. Circuits and Systems for Video Technology*, vol. 7, no. 4, pp. 433-437, April 1997.
- [25] Yang, Y., N.P. Galatsanos, and A.K. Katsaggelos, "Regularized reconstruction to reduce blocking artifacts of block discrete cosine transform compressed images", *IEEE Trans. Circuits and Systems for Video Technology*, vol. 3, no. 6, pp. 421-432, December 1993.
- [26] Yang, Y., N.P. Galatsanos, and A.K. Katsaggelos, "Projection-based spatially adaptive reconstruction of block-transform compressed images", *IEEE Trans. Image Process.*, vol. 4, no. 7, pp. 896-908, July 1995.

<sup>1</sup>In order to replicate the experiments as in [1], the "Peppers" image used for Table 2 is the green channel of the RGB color Peppers. Let us note, however, that far more often in the literature the grayscale Peppers is found as the luminance channel Y of the RGB Peppers image.